

Modeling stochastic Ca^{2+} release from a cluster of IP_3 -sensitive receptors

L. Diambra

Instituto de Física de São Carlos, Universidade de São Paulo,
Caixa Postal: 369, cep: 13560-970, São Carlos SP, Brazil.
diambra@if.sc.usp.br

Abstract

We focused our attention on Ca^{2+} release from the endoplasmic reticulum through a cluster of inositol 1,4,5-trisphosphate (IP_3) receptor channels. The random opening and closing of these receptors introduce stochastic effects that have been observed experimentally. Here, we present a stochastic version of Othmer-Tang model for IP_3 receptor clusters. We address the average behavior of the channels in response to IP_3 stimuli. We found, by stochastic simulation, that the shape of the receptor response to IP_3 (fraction of open channels versus $[\text{IP}_3]$), is affected by the cytosolic Ca^{2+} level. We also study several aspects of the stochastic properties of Ca^{2+} release and we compare with experimental observations.

1 Introduction

Ionized calcium (Ca^{2+}) not only represents the most common signal transduction element relaying information within cells to control a wide array of activities including secretion, contraction and cell proliferation, but also is invariably involved in cell death (Berridge, 1997). To coordinate all of these functions, cytosolic Ca^{2+} needs to be precisely regulated in space, time and amplitude. Normal concentrations of cytosolic Ca^{2+} ($[\text{Ca}^{2+}] \sim 100 \text{ nM}$) is 20000 fold lower than the 2 mM concentration found extracellularly. Under resting conditions this gradient is maintained by active extrusion of cytosolic Ca^{2+} by Ca^{2+} ATPases present in the plasma membrane and in the endoplasmic reticulum (ER), or in the sarcoplasmic reticulum in electrically excitable cells. These pumps counterbalance the leak of Ca^{2+} into the cytosol from both the extracellular space and the ER Ca^{2+} store.

A wide variety of extracellular stimuli cause the increase of $[\text{Ca}^{2+}]$ to exert their effect. In non-excitabile cells, this increase is triggered by inositol(1,4,5)-trisphosphate (IP_3), produced upon activation of phospholipase C (Berridge, 1997). IP_3 rapidly diffuses into the cytosol, where it interacts with the inositol(1,4,5)-trisphosphate receptors (IP_3R), to promote the release of Ca^{2+} into the cytosol. Depending on the cell type, the resulting cytosolic Ca^{2+} signal can have a complex spatio-temporal composition (Berridge, 1997). It is generally recognized that, in the presence of a constant external stimulus, the Ca^{2+} displays spiking behavior. These Ca^{2+} oscillations can be spatially localized or extended, spreading as a wave throughout the entire cell.

The process of Ca^{2+} released from the ER through channels is nonlinear since, increased Ca^{2+} concentration in the cytosol favors channel opening. This autocatalytic amplification is called calcium-induced calcium release (CICR). There are a variety of channels showing CICR. Ca^{2+} release is terminated by closure of the channels at high Ca^{2+} levels, after which Ca^{2+} is removed from the cytosol by the action of the Ca^{2+} ATPases.

It has been observed that Ca^{2+} release channels are spatially organized in clusters. Single release channel, named Ca^{2+} blips, has been observed in experiments (Bootman et al., 1997). Collective opening and closing of several Ca^{2+} channels in a cluster, named puffs, have also been observed in experiments (Callamaras et al., 1998). That suggests a hierarchy of calcium signaling events from small blips to large puffs (Lipp and Niggli, 1998; Bootman et al., 1997). Improved spatial and temporal resolution in recording reveal that there is not a clear distinction between fundamental blips and elementary puffs. Channels open and close in a stochastic way. Ca^{2+} release by one channel increase the open probability for the neighboring channels. Thus at high levels of IP_3 , neighboring clusters become functionally coupled by Ca^{2+} diffusion and CICR support the formation of spatiotemporal patterns of intracellular Ca^{2+} release.

Watrás et al. (1991) found that Ca^{2+} channels in the cerebellum exhibits four conductance levels that are multiples of a unit conductance step. This observation suggests that the number of interacting receptors in one complex can vary from one to four and supports the hypothesis

that the channel is a tetramer. Examination of the IP_3 dependence of channel, yielded Hill coefficients of 1-1.3 (Watrass et al., 1991). However, in hepatocytes the response to IP_3 are positively cooperative with a Hill coefficient of 3.0-3.4 (Marchant and Taylor, 1997; Dufour et al., 1997) or. In our numerical simulation we found that the Hill coefficient increase from 1.15 to 2.2 when total Ca^{2+} (cytosolic + stored) level increase. However, the model is not able to explain higher values of n_h as that reported by Marchant and Taylor (1997). This finding suggest that feedback from cytosolic Ca^{2+} plays a key role in the channel response to IP_3 , but is not able to explain high Hill coefficients found in some tissues.

Experimental finding of Bezprozvanny et al. (1991) clear up several aspects of the kinetic of the receptors. Thus several models for Ca^{2+} dynamics in systems involving IP_3R have been proposed (De Young and Keizer, 1992; Othmer and Tang, 1993; Bezprozvanny and Ehrlich, 1994). These models of IP_3R assume a regulatory site for IP_3 on the channel complex, one activating site and one inhibiting site for Ca^{2+} . Experimental findings suggest that the channel is open when IP_3 ion is bound to its corresponding domain and Ca^{2+} is bound to its activating domain and not bound to its inhibiting site. In the aforementioned models, Ca^{2+} binding to the activating regulatory site is a fast process compared with that of inhibiting binding and all these models reproduce a bell-shaped curve when one plots the fraction of open channels as a function of $\log[\text{Ca}^{2+}]$.

De Young and Keizer model (DKM) for IP_3R assumes that the ligands can bind to any unoccupied site on the IP_3R independently of the binding status of the other sites, which leads to eight possible states of the receptor (De Young and Keizer, 1992). A more general scheme is to assume state-dependent binding to each site. In this framework, the simplest model was developed by Othmer and Tang (1993) which assumes that the binding order of ions and molecules to the receptor is not free. In the Othmer-Tang model (OTM) it is assumed that the binding process is sequential (Othmer and Tang, 1993). Ca^{2+} binds to the activating site on the receptor only after IP_3 has bound, and that the binding of calcium to inhibitory site occurs only after calcium is bound to the activating site. This sequential binding leads to four possible states for the receptor. Bezprozvanny and Ehrlich (1994) proposed a variation to the OTM which incorporates an additional closed state corresponding to activating site occupied which decay rapidly to the open state.

The bindings of IP_3 and Ca^{2+} to the regulatory sites are stochastic events rendering the opening and closing of the channel a stochastic process. The small number of calcium channels in a cluster indicates that deterministic models might be insufficient. In fact, abortive waves cannot be understood in terms of deterministic models, since in these models an excitation travels steadily if it travels at all. The stochastic effects are relevant for modeling Ca^{2+} wave propagation. Furthermore, the observation of localized stochastic Ca^{2+} puffs and the rather small number of channels creating the localized event, suggest that it is mandatory take into account the binding processes as stochastic events. The stochastic dynamics of clustered IP_3R has been studied by Swillens et al. (1999) which model has 14 states. There are also several studies considering stochastic dynamics focusing on the onset of the saltatory propagation of

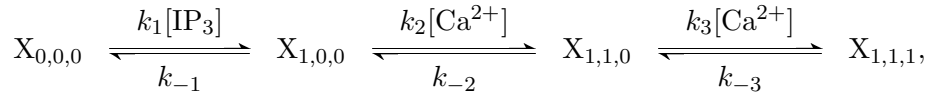
calcium waves due to intercluster diffusion of Ca^{2+} (Keizer et al., 1998; Falcke et al., 2000). Shuai and Jung (2002b) have been study the statistical properties of Ca^{2+} release in a stochastic and simplified version of the DKM.

In this paper we regard a Markov-stochastic version of the OTM to study the stochastic properties of the calcium release of IP_3R clusters. We decided to stick to the Othmer and Tang approach because the OTM has the least number of channel states and kinetic parameters, yet it adequately explains the experimentally observed channel kinetics. After a brief description of the model in Section 2, we discuss the role of cytosolic calcium and IP_3 in regulating the fraction of open channels. We show that the fraction of open channels versus IP_3 concentration fit a Hill curve which coefficient increase with the average intracellular calcium concentration. The amplitude, inter-puff interval (IPI) and size distribution of calcium puffs are also discussed. Finally, we show that there are no correlation between two consecutive IPIs, but there are some correlation between the puff duration and the puff amplitude.

2 Materials and Methods

2.1 Stochastic version of OTM

In the Othmer and Tang model there is only one subunit/receptor in a each channel. The three binding sites on the receptor and the sequential binding scheme allows four different states for the receptor $X_{i,j,k}$. The index i stands for the IP_3 site, j for the activating Ca^{2+} site, and k for the inhibiting Ca^{2+} . An index is 1 if an ion is bound and 0 if not. The state transition scheme is given by the pathway



in which the k_i , $i = \pm 1, \pm 2, \pm 3$, are the rate constant of the state transitions. The channel is only conductive when the receptor is in the state $X_{1,1,0}$. The channels are assumed to be close enough so that Ca^{2+} concentrations can be considered homogeneous throughout the cluster. We neglect Ca^{2+} diffusion between cluster and environment without accounting for spatial aspects of formation and collapse of Ca^{2+} waves. We will not consider calcium transport across the plasma membrane. Thus the Ca^{2+} simply flow or is pumped back and forth between the ER and the cytoplasm, and the total intracellular calcium concentration is constant. Thus, the dynamic of Ca^{2+} in the cytoplasm is governed by the equation

$$\frac{d[\text{Ca}^{2+}]}{dt} = J_{channel} + J_{leak} - J_{pump}, \quad (1)$$

where $J_{channel}$ is the calcium flux from the ER to the cytoplasm through the IP_3R channel, J_{pump} is the calcium flux pumped from the cytoplasm into ER, and J_{leak} is the calcium flux

being leakage from the ER to the cytoplasm. The expression for the fluxes are given by

$$\begin{aligned}
J_{channel} &= v_r \gamma_1 \frac{N_{open}}{N} ([Ca^{2+}]_{ER} - [Ca^{2+}]) \\
J_{leak} &= v_r \gamma_0 ([Ca^{2+}]_{ER} - [Ca^{2+}]) \\
J_{pump} &= \hat{p}_1 \frac{[Ca^{2+}]^4}{[Ca^{2+}]^4 + \hat{p}_2^4},
\end{aligned} \tag{2}$$

where v_r is the ratio of the ER volume to the cytoplasm volume, γ_1 is the maximal Ca^{2+} fluxes. N_{open} is a random variable that represent the number of channels open (receptors in the state $X_{1,1,0}$) and N is the total number of channels in the receptor. γ_0 is the basal permeability of the ER membrane in the absence of IP_3 . For the study of Ca^{2+} dynamics in many cell types, Ca^{2+} exchange with the extracellular medium is much smaller than the Ca^{2+} flux across the ER membrane (Koster et al., 1993; Thastrup, 1990). For this reason, Eqs. (1-2) can be simplified by using the volume average intracellular calcium concentration $[Ca^{2+}]_{ave} = ([Ca^{2+}] + v_r [Ca^{2+}]_{ER}) / (1 + v_r)$. The $[Ca^{2+}]_{ave}$ is a control parameter whose value we can choose, but that it is not a dynamical variable. We then define $C = [Ca^{2+}] / [Ca^{2+}]_{ave}$ and rewrite the Eqs. (1-2) in the form

$$\dot{C} = (1 + v_r) (\gamma_0 + \gamma_1 N_{open}) (1 - C) - p_1 \frac{C^4}{C^4 + p_2^4}, \tag{3}$$

where $p_1 = \hat{p}_1 / [Ca^{2+}]_{ave}$ and $p_2 = \hat{p}_2 / [Ca^{2+}]_{ave}$.

This equation was numerically integrated using fourth order Runge-Kutta algorithm, with the actual configuration of open channels N_{open} , which is obtained from stochastic simulations of the kinetics of the receptors. The number of open channels changes due to six stochastic processes: the IP_3 binding (unbinding) to (from) receptors; the activation (deactivation) of receptors by binding (unbinding) Ca^{2+} to (from) their activation domains; the inhibition (activation) of receptors by binding (unbinding) Ca^{2+} to (from) their inhibition domains. Transitions involving binding (but not those involving unbinding) depend on the concentration of IP_3 or Ca^{2+} . Let us define the probability distribution vector $\mathcal{P}(t) = (P_{0,0,0}(t), P_{1,0,0}(t), P_{1,1,0}(t), P_{1,1,1}(t))^T$, where $P_{i,j,k}$ denotes the probability that the receptor is in the state $X_{i,j,k}$. The dynamic of the vector $\mathcal{P}(t)$ is described by the master equation,

$$\dot{\mathcal{P}} = Q\mathcal{P}, \tag{4}$$

where Q represents a (4×4) matrix of transition probabilities,

$$Q = \begin{pmatrix} 1 - k_1 [IP_3] & k_{-1} & 0 & 0 \\ k_1 [IP_3] & 1 - k_{-1} - k_2 [Ca^{2+}] & k_{-2} & 0 \\ 0 & k_2 [Ca^{2+}] & 1 - k_{-2} - k_3 [Ca^{2+}] & k_{-3} \\ 0 & 0 & k_3 [Ca^{2+}] & 1 - k_{-3} \end{pmatrix}, \tag{5}$$

For the stochastic part of the simulation, the state of each receptors at time $t + \Delta t$ were independently updated from the previous state and Q . If the time step Δt is sufficiently small

to allow at most one transition, the probabilities for the receptor to transform into the various possible states within this short time interval are given by

$$\begin{aligned}
P_{0,0,0 \rightarrow 1,0,0} &= k_1 [\text{IP}_3] \Delta t & P_{1,0,0 \rightarrow 0,0,0} &= k_{-1} \Delta t \\
P_{1,0,0 \rightarrow 1,1,0} &= k_2 [\text{Ca}^{2+}] \Delta t & P_{1,1,0 \rightarrow 1,0,0} &= k_{-2} \Delta t \\
P_{1,1,0 \rightarrow 1,1,1} &= k_3 [\text{Ca}^{2+}] \Delta t & P_{1,1,1 \rightarrow 1,1,0} &= k_{-3} \Delta t.
\end{aligned} \tag{6}$$

For this model, there is only one possible transition out of the states $X_{0,0,0}$ and $X_{1,1,1}$, while there are two possible transitions out of the states $X_{1,0,0}$ and $X_{1,1,0}$. In the last case a random number ρ between 0 and 1 was drawn from a uniform distribution for each update step. Then, a channel initially in state, for example, $X_{1,0,0}$, will be updated to state $X_{1,1,0}$, if $\rho < P_{1,0,0 \rightarrow 1,1,0}$, and to state $X_{0,0,0}$ if $P_{1,0,0 \rightarrow 1,1,0} < \rho \leq P_{1,0,0 \rightarrow 0,0,0} + P_{1,0,0 \rightarrow 1,1,0}$, and remained in its current state otherwise.

All over the paper we have used $\Delta = 0.001$ s, and the number of receptors in a cluster, N , was set to 20. This number is based on the theoretical predictions of the cluster size by Swillens et al. (1999), from numerical studies regarding the requirements of interchannel communication. Furthermore, found that the optimal cluster size for coherence resonance is around $N = 20$ (Shuai and Jung, 2002a). The values of the parameters for the kinetic model used in this paper are given in Table 1.

To observe puffs in experiments, calcium diffusion is suppressed by intracellular loading with the Ca^{2+} buffer EGTA (Thomas et al., 1998; Marchant et al., 1999; Cheng et al., 1999; Callamaras and Parker, 2000). With a large loading of EGTA, the clusters become functionally isolated (Callamaras and Parker, 2000). Under these condition, our model is valid.

3 Results

3.1 The channel response to IP_3 and Ca^{2+}

Before to study the statistical properties of the intracellular Ca^{2+} release, we firstly address the average behavior of channels in response to IP_3 stimuli. In this sense, we simulate the stochastic dynamics (Eq. 4-5) with the parameters in Table 1 and using $[\text{Ca}^{2+}]_{ave}$ as control parameter. We compute the mean value of cytosolic Ca^{2+} concentration in a long time period (10,000 seconds) as a function of $[\text{IP}_3]$ for several values of $[\text{Ca}^{2+}]_{ave}$ (0.4, 0.8, 1.2, 1.6, 1.9 and 2.4 μM). The results are sigmoidal curves as is shown in Fig. 1. It should be noted that the cytosolic mean Ca^{2+} invariably increases with the level of $[\text{Ca}^{2+}]_{ave}$. The vertical grey lines both in Fig. 1 and Fig. 2 are indicating the IP_3 levels for which we have also studied several statistical properties of the puffs. Further insight can be obtained computing the effect of the IP_3 over the mean fraction of open channels. The mean fraction of channel that is activated increase monotonically as the IP_3 level increases following Hill curves ($r^2 \geq 0.995$ in all cases)

as shown in the Fig. 2. The Hill curve is defined by

$$\frac{N_{open}}{N} = V_{max} \frac{[IP_3]^{n_h}}{k^{n_h} + [IP_3]^{n_h}}, \quad (7)$$

where k is the half maximal value, V_{max} is the maximum fraction of channels open, and n_h is Hill coefficient. In the top panel of Fig. 3 we depict the Hill coefficient n_h and in the bottom panel we depict k and V_{max} for different values of $[Ca^{2+}]_{ave}$. The Hill coefficient increases as $[Ca^{2+}]_{ave}$ increases. At physiological values of $[Ca^{2+}]_{ave}$, the n_h found in our simulation range from 1.15 to 2.2 in very well agreement with the experimental values which range from 1.0 (Volpe et al., 1990) to greater than 3.7 (Delisle, 1991). In the bottom panel of Fig. 3 we depict the others two fitted parameters V_{max} and k . The maximum fraction of open channels V_{max} are between $[0.15, 0.30]$ with a maximum at 0.80 of $[Ca^{2+}]_{ave}$, this range is slightly higher than the values found by Watras et al. (1991), around 0.14 in cerebellar cells (with $n_h = 1.3$). It should be noted that the half-maximal k decrease with the level of $[Ca^{2+}]_{ave}$ and range from 0.10 to 0.7 μM IP₃. The half-maximal found in the Watras experiment was 0.15 μM IP₃.

Bezprozvanny et al. (1991) shown, in experiment where Ca^{2+} channels reconstituted in lipid bilayers, that the fraction of open channel as a function of $\log[Ca^{2+}]$ has an asymmetry bell-shaped curve, in experiment where calcium was clamped. The mathematical analysis of the master equation (4), allows to determine the open channel probability (to find the receptor in the state $X_{1,1,0}$) for a given $[Ca^{2+}]$ and $[IP_3]$. The steady-state distribution vector \mathcal{P}^{st} correspond to the normalized eigenvector associated to the eigenvalue zero of the equation of (4). Some algebraic manipulations lead to

$$P_{1,1,0}^{st}([IP_3], [Ca^{2+}]) = \frac{K_1 K_2 [IP_3] [Ca^{2+}]}{1 + K_1 [IP_3] + K_1 K_2 [IP_3] [Ca^{2+}] + K_1 K_2 K_3 [IP_3] [Ca^{2+}]^2}, \quad (8)$$

where $K_1 = k_1/k_{-1}$, $K_2 = k_2/k_{-2}$ and $K_3 = k_3/k_{-3}$. Fig. 4 depicts the open channel probability for three different values of IP₃ concentration as a function of $[Ca^{2+}]$. The result (8) predicts the bell-shaped curve obtained experimentally by Bezprozvanny et al. (1991), with the symmetry axe correctly shifted to left. It should be noted the difference between Eq. (7) and (8). The first one can be understood as a open channel probability in physiological conditions described by Eq. (1-2). Thus the fraction of open channels is computed as the average of fraction of open channels over a period of time (10,000 seconds in this paper), where calcium is released (removed) to (from) cytosol many times. On the other hand, Eq. (8) is a steady state probability for a fix level of calcium and IP₃. This situation emulate the Bezprozvanny et al. experimental conditions, where the calcium was clamped.

3.2 Statistical properties of puffs

We now study the statistical properties of puffs obtained with the stochastic version of the OTM, the deterministic version of OTM is not able to address these properties. It is known that IP₃

stimuli evokes repetitive spikes in the intracellular $[Ca^{2+}]$ rather than simply increase $[Ca^{2+}]$. In the Fig. 5, we can see the typical spiking behavior of calcium release by a cluster with 20 channels ($N = 20$) and some statistical properties of the observed puffs 10,000 seconds of simulations. In this case, we performed the simulation setting $[Ca^{2+}]_{ave}=1.6 \mu M$ and $IP_3=0.35 \mu M$. At the top panel of Fig. 5 we depict the first 100 seconds of the temporal course of the intracellular calcium concentration. At the bottom-left panel, the scatter plot of IPI_i versus IPI_{i+1} shown that there is not temporal correlation between two consecutive IPIs. At the bottom-center panel: scatter plot of puff amplitude versus puff duration shown that there is correlation between puff amplitudes and durations ($r^2=0.84$). Small puff amplitudes are correlated with brief puffs, the correlation decreases as amplitude puff increases. Experimental observations of Thomas et al. (1998) indicate similar correlations, but with a smaller linear regression coefficient ($r^2=0.69$). At the bottom-right panel we shown the puff size distribution, it should be noted that there are Ca^{2+} releases of all sizes. All plots in the bottom panel of Fig. 5, and hereafter, were computed with puffs which amplitudes exceed the threshold $0.20 \mu M$, in order to avoid the background fluctuation. In this paper, the puff size is defined as the area between the $[Ca^{2+}]$ time course and the threshold.

It was experimentally established that when the IP_3 concentration increases, the mean frequency of spiking raises, but the amplitude remain essentially constant. Fig. 6 displays the mean frequency of puffs as a function of the IP_3 concentration for the some values of $[Ca^{2+}]_{ave}$ showed in Figs. 1-2 ($0.8, 1.2, 1.6, 1.9$ and $2.4 \mu M$) obtained by stochastic simulations. We can observe that the onset of spiking behavior in response to the IP_3 stimuli depends on the $[Ca^{2+}]_{ave}$. For high levels of calcium, even low levels of IP_3 are able to produce repetitive puffs. These responses are well characterized by Hill curves. The Hill coefficients associated to these curves were essentially independent of $[Ca^{2+}]_{ave}$ level. For $[Ca^{2+}]_{ave}=2.4 \mu M$ the Hill coefficient was 2.1 and decrease to 1.8 for $[Ca^{2+}]_{ave}=0.8 \mu M$.

Furthermore, the number of channel recruited in the puffs varies stochastically from puff to puff. Important, and experimentally recorded, characteristics of these variabilities are amplitude, inter-puff interval, duration and size distributions (Bootman et al., 1997; Sun et al., 1998; Thomas et al., 1998; Callamaras and Parker 2000; Marchant and Parker 2001). The shape of the puff amplitude distribution depends on the concentration of IP_3 and the $[Ca^{2+}]_{ave}$. In Fig. 7 we shown a diagram of the puff amplitude distributions in the $[Ca^{2+}]_{ave}$ - IP_3 plane. In order to comparison the scale of the axis are the same for all plots in the diagram, between $[0.20,1.80] \mu M$ for the amplitudes of puffs (horizontal axe), and between $[0,6000]$ for the number of events (vertical axe). No events (NE) were recorded for $[IP_3]= 0.07 \mu M$ and low level of $[Ca^{2+}]_{ave}=0.8 \mu M$. For lower $[Ca^{2+}]_{ave}$, the amplitudes of the spontaneous puffs are typically smaller than $0.20 \mu M$ and are regarded as fluctuations. For $[Ca^{2+}]_{ave}=0.8 \mu M$, or $[IP_3]= 0.07 \mu M$, monotonically decreasing amplitude distribution are found. In the other cases a two-peak amplitude distributions are mainly found. The characteristic amplitudes depend on $[Ca^{2+}]_{ave}$, but not on $[IP_3]$. For $[Ca^{2+}]_{ave}=1.6 \mu M$, the typical amplitude was around $0.80 \mu M$. The shape of the puff amplitude distributions shown in the Fig. 7 differ from those observed in experiments, which have one-peak shape (Sun et al., 1998; Thomas et al., 1998; Marchant and Parker,2001).

Another important characteristic of the calcium dynamics is the distribution of time interval between two consecutive puffs. Recent experimental investigation with *Xenopus* oocytes has revealed that IPI distribution exhibits a single peak. In Fig. 8 we display another diagram in the $[\text{Ca}^{2+}]_{ave}$ -IP₃ plane, but now with IPI distributions. In this diagram the range of the vertical axis are the same for all distributions, between [0,6000] events. While the ranges of IPI (horizontal axis) are between [0,80] seconds for the first column ($[\text{Ca}^{2+}]_{ave} = 0.8 \mu\text{M}$), and between [0,20] seconds for all other cases. For $[\text{Ca}^{2+}]_{ave} = 0.8 \mu\text{M}$, the IPI distribution seems to decay exponentially. However, when the level of $[\text{Ca}^{2+}]_{ave}$ is increased, skewed single-peak distribution characterize the IPI distributions. The position of the single peak range from 1 to 2 seconds increasing with the $[\text{Ca}^{2+}]_{ave}$. The shape of the distributions shown in the Fig. 8 are consistent with observed by Marchant et al. (1999), but with a typical IPI smaller than that observed in the experiment (around 2.5 seconds). It is apparent that for high values of [IP₃] and $[\text{Ca}^{2+}]_{ave}$, the IPI are quite regular.

We also want to illustrate the typical temporal behavior and some statistical properties, as we shown in the Fig. 5, for two different situations: i) high [IP₃], low $[\text{Ca}^{2+}]_{ave}$ (Fig. 9); and ii) low [IP₃], high $[\text{Ca}^{2+}]_{ave}$ (Fig. 10). It should be noted that different scale axis were used. In Fig. 9, where [IP₃]=21 μM , and $[\text{Ca}^{2+}]_{ave}=0.8 \mu\text{M}$, we found the distribution of puffs size decay exponentially, and there are very few great calcium release events (bottom-right panel). More broad distributions of IPI are yielded for this case than those shown in bottom-left panel of Figs. 5 and 10. There are also less IPI around 1-2 seconds (bottom-left panel) than those shown in Fig. 5 or in Fig. 10. The correlation between puff amplitude and duration seems to be similar than that shown in bottom-right panel of Fig. 5. When increase the $[\text{Ca}^{2+}]_{ave}$ until 2.4 μM and decrease the [IP₃] to 0.07 μM (Fig. 10), we found a slower exponential decay in the distribution of puffs size than in Fig. 9 (bottom-right panel). In this case the distributions of IPI (bottom-center panel of Fig. 10) looks like those shown in bottom-left panel of Figs. 5. Puff with small amplitude seems to be correlated with short duration.

4 Discussion and conclusion

We have developed a stochastic version of the Othmer-Tang model to study dynamical and statistical properties of Ca^{2+} release of clusters of IP₃-sensitive receptors. In comparison to others stochastic models (Falcke et al., 2000; Bär et al., 2000; Swillens et al., 1999), our receptor model is simpler and is represented by only four states. In this stochastic clustered IP₃R model, the Ca^{2+} diffusion between the cluster and the environment is ignored so that an isolated cluster can be discussed. However, the channels are assumed to be close enough and the instantaneous Ca^{2+} diffusion within a cluster is so fast that the calcium concentration within a cluster is always homogeneous.

We found that the model reproduce experimental result by Watras et al. (1991) where it is shown that the channel response to the IP₃ follow a Hill curve. In intact cells, the long latency

and subsequent sigmoidal increase in cytosolic $[Ca^{2+}]$ after addition of agonists (Berridge, 1997), are consistent with either positively cooperative activation of IP_3 Rs by IP_3 alone or by feedback from cytosolic $[Ca^{2+}]$. Distinguishing between these mechanisms, however, is difficult in intact cells, in which IP_3 receptor activation inevitably increases cytosolic $[Ca^{2+}]$. In broken cells, the use of fluorescent indicators to measure rapid rates of Ca^{2+} efflux is prone to similar difficulties. Results from a variety of tissues using superfusion (Finch et al., 1991), bilayer recording (Watras et al., 1991; Besprozvanny et al., 1991), fluorescent indicators (Champeil et al., 1989) or flash photolysis of caged IP_3 in intact cells (Parker et al., 1996) suggest that responses to IP_3 are either not positively cooperative (Finch et al., 1991; Parker et al., 1996; Watras et al., 1991) or only slightly so (Besprozvanny et al., 1991; Champeil et al., 1989). Each approach has its limitations and together the results provide no clear indication of whether responses to IP_3 are positively cooperative in the absence of positive feedback from cytosolic Ca^{2+} . In our numerical simulation we found that, even in absence of cooperativity in the model, the Hill coefficient increase from 1.15 to 2.2 when $[Ca^{2+}]_{ave}$ increase. However, the model is not able to explain higher values of n_h as that reported by Marchant and Taylor (1997). This results suggest that feedback from cytosolic Ca^{2+} plays a key role in the channel response to IP_3 , but to explain high values of n_h found in some tissues, a cooperative mechanism could be mandatory.

Other important aspect is the frequency encoding. It is well known that IP_3 stimuli evoke repetitive spikes in the intracellular Ca^{2+} concentration rather than simply elevating the level of Ca^{2+} . Moreover, when the $[IP_3]$ is increased, the mean frequency of spiking raises, but the amplitude remains essentially constant. Thus a continuous level of stimuli signal is converted into a frequency-encoded signal: the number of spikes per time unit (Tang and Othmer, 1995). A common problem found in this kind of converter devices is the competition between two desirable goals: i) high sensitivity, the system ideally should be able to detect even weak signals; and ii) large dynamic range, the system should not saturate over various orders of magnitude of input intensity. For this reason the Hill coefficient (when the response is well-fitted by a Hill curve) its desirable to be less than 1. In the results derived from our numerical simulation, we can observe that the mean frequency of the spiking behavior in response to the IP_3 stimuli is well characterized by Hill curves. The Hill coefficient, between 1.8-2.1, was essentially independent of $[Ca^{2+}]_{ave}$. This value is too high given narrow dynamical range in order to frequency-encode the IP_3 signal. However, this narrow dynamical range observed in isolated cluster, could be translates into a wider dynamical range as result of the collective phenomenon by considering an intercluster communication mechanism. This interesting discussion is the subject of our current research and will be discussed in a forthcoming paper.

The small number of the IP_3 Rs in a cluster introduce stochastic oscillation into the calcium release dynamics. Experimental data suggest that the localized calcium release varies in a continuous fashion due to stochastic variation in both numbers of channels recruited and durations of channel openings. It is not obvious which aspects of Ca^{2+} puffs are originally determined by the dynamics of the Ca^{2+} channels, which properties are determined by the diffusion and Ca^{2+} binding kinetics, and which properties are induced from the measurement procedures (Cheng et al., 1999; Izu et al., 1998). Although in several experiments one-peak amplitude distributions

were observed, Cheng et al., (1999) suggested that the original calcium puffs should have an exponential decaying decreasing amplitude distribution. Our stochastic simulations shown that the amplitude distributions varies in a continuous fashion from exponential decay to two-peak distributions. Even for a small threshold (as $0.20 \mu\text{M}$) a peak is observed in the amplitude distributions for high values both of $[\text{IP}_3]$ and $[\text{Ca}^{2+}]_{ave}$. However, the puffs size (i.e. amplitude \times duration) distributions have essentially an exponential decay distribution over the range studied here. These results indicate that a fixed puff morphology which is sometimes assumed in literature (Pratusevich and Balke, 1996; Izu et al., 1998; Cheng et al., 1999) is not a good assumption for Ca^{2+} puff analysis. Furthermore, in our markovian simulation, we found that the amplitude of puff is correlated with its duration in agreement with experimental observation reported by Thomas et al., (1998).

Other useful way to characterize the calcium puffs dynamics is using the IPI distributions. The stochastic simulation of the OTM shown that the IPI distributions varies from exponential decay to a skewed bell-shape distributions. For physiological values of IP_3 and $[\text{Ca}^{2+}]_{ave}$ the distributions have a maximum around 1.5 seconds. The shape is consistent with distribution observed by Marchant et al. (1999), however, the typical IPI observed in the experiment, around 2.5 seconds, was slightly higher. In contrast to the deterministic models, we shown that two consecutive IPI are not correlated. For this reason, the random spiking behavior or stochastic oscillations have an essentially different nature that the periodic oscillations generated by deterministic models.

We want to remark that the stochastic oscillations are different from the stochastic excitability discussed by Keizer and Smith (1998). For the stochastic excitability, once $[\text{Ca}^{2+}]$ randomly becomes larger than a threshold, a fast release (action-potential-like) of $[\text{Ca}^{2+}]$ followed by a refractory period can be observed. For the stochastic oscillation studied here there is not such a threshold. More broad distributions of puff amplitudes and IPI are yielded for stochastic oscillation.

Acknowledges

This research was partially supported by the Deutsche Forschungsgemeinschaft. The author thanks to Gerhard Thiel and Nara Guisoni for valuable suggestions. L.D. is grateful for the hospitality of Professor Friedemann Kaiser and Nonlinear Dynamics Group at the Darmstadt University of Technology where these ideas were developed.

References

Bär, M., M. Falcke, H. Levine, and L. S. Tsimring. 2000. Discrete stochastic modeling of calcium channel dynamics. *Phys. Rev. Lett.* 84:5664-5667.

- Berridge, M. J., 1997. Elementary and global aspect of calcium signaling. *J. Physiol.* 499:291-306.
- Bezprozvanny, I., J. Watras, and B. Ehrlich. 1991. Bell-shaped calcium response curves of Ins(1,4,5)P₃- and calcium-gated channels from endoplasmic reticulum of cerebellum. *Nature.* 351:751-754.
- Bezprozvanny, I., and B. E. Ehrlich. 1994. Inositol 1,4,5-trisphosphate (IP₃)-gated Ca channels from cerebellum: conduction properties for divalent cations and regulation by intraluminal calcium. *J. Gen. Physiol.* 104:821-856.
- Bootman, M., E. Niggli, M. Berridge, and P. Lipp. 1997. Imaging the hierarchical Ca²⁺ signaling system in HeLa cells. *J. Physiol.* 499:307-314.
- Callamaras, N., J. S. Marchant, X. Sun, and I. Parker. 1998. Activation and co-ordination of InsP₃-mediated elementary Ca²⁺ events during global Ca²⁺ signals in *Xenopus* oocytes. *J. Physiol.* 509:81-91.
- Callamaras, N., and I. Parker. 2000. Phasic characteristic of elementary Ca²⁺ release sites underlies quantal responses to IP₃. *EMBO J.* 19:3608-3617.
- Champeil, P., L. Combettes, B. Berthon, E. Doucet, S. Orlowski, M. Claret. 1989. Fast kinetics of calcium release induced by myo-inositol trisphosphate in permeabilized rat hepatocytes. *J. Biol. Chem.* 264:17665-17673.
- Cheng, H., L. Song, N. Shirokova, A. Gonzalez, E. G. Lakatta, E. Rios, and M. D. Stern. 1999. Amplitude distribution of calcium sparks in confocal images: theory and studies with an automatic detection method. *Biophys. J.* 76:606-617.
- Delisle, S. 1991. The four dimensions of calcium signaling in *Xenopus* oocytes. *Cell Calcium.* 12:217-227.
- De Young, G. W., and J. Keizer. 1992. A single-pool inositol 1,4,5- trisphosphate-receptor-based model for agonist-stimulated oscillations in Ca²⁺ concentration. *Proc. Natl. Acad. Sci. USA.* 89:9895-9899.
- Dufour, J. F., I. M. Arias, and T. J. Turner. 1997. Inositol 1,4,5-trisphosphate and calcium regulate the calcium channel function of the hepatic inositol 1,4,5-trisphosphate receptor. *J. Biol. Chem.* 272:2675-2681.
- Falcke, M., L. Tsimring, and H. Levine. 2000. Stochastic spreading of intracellular Ca²⁺ release. *Phys. Rev. E.* 62:2636-2643.
- Finch, E.A., T.J. Turner, S. M. Goldin. 1991. Calcium as a coagonist of inositol 1,4,5-trisphosphate-induced calcium release. *Science.* 252:443-446.
- Izu, L. T., W. G. Wier, and C. W. Balke. 1998. Theoretical analysis of the Ca²⁺ spark amplitude distribution. *Biophys. J.* 75:1144-1162.

- Keizer, J., and G. D. Smith. 1998. Spark-to-wave transition: saltatory transmission of calcium waves in cardiac myocytes. *Biophys. Chem.* 72:87-100.
- Keizer, J., G. D. Smith, S. Ponce-Dawson, and J. E. Pearson. 1998. Saltatory propagation of Ca^{2+} waves by Ca^{2+} sparks. *Biophys. J.* 75:595-600.
- Koster, H., C. van Os, and R. Bindels. 1993. Ca^{2+} oscillations in the rabbit renal cortical collecting system induced by Na^+ free solutions. *Kidney Int.* 43:828-836.
- Lipp, P., and E. Niggli. 1998. Fundamental calcium release events revealed by two-photon excitation photolysis of caged calcium in guinea-pig cardiac myocytes. *J. Physiol.* 508:801-809.
- Marchant, J. S., and C. W. Taylor. 1997. Cooperative activation of IP_3 and Ca^{2+} safeguards against spontaneous activity. *Current Biology* 7:510-518.
- Marchant, J. S., N. Callamaras, and I. Parker. 1999. Initiation of IP_3 -mediated Ca^{2+} waves in *Xenopus* oocytes. *EMBO J.* 18:5285-5299.
- Marchant, J. S., and I. Parker. 2001. Role of elementary Ca^{2+} puffs in generating repetitive Ca^{2+} oscillations. *EMBO J.* 20:65-76.
- Othmer, H. G., and H. Tang. 1993. In Oscillations and waves in a model of calcium dynamics. *In* Experimental and Theoretical Advances in Biological Pattern Formation. H. Othmer, J. Murray, and P. Maini, editors. Plenum Press, London. 295-319,
- Parker, I., Y. Yao, V. Ilyin. 1996. Fast kinetics of calcium liberation induced in *Xenopus* oocytes by photoreleased inositol trisphosphate. *Biophys J.* 70:222-237.
- Pratusevich, V. R., and C. W. Balke. 1996. Factors shaping the confocal image of the calcium spark in cardiac muscle cells. *Biophys. J.* 71:2942-2957.
- Shuai, J. W., and P. Jung. 2002a. Optimal intracellular calcium signaling. *Phys. Rev. Lett.* 88:68102-1-68102-4.
- Shuai, J. W., and P. Jung. 2002b. Stochastic properties of Ca^{2+} release of inositol 1,4,5-trisphosphate receptor cluster. *Biophys. J.* 83:87-97.
- Sun, X., N. Callamaras, J. S. Marchant, and I. Parker. 1998. A continuum of InsP_3 -mediated elementary Ca^{2+} signaling events in *Xenopus* oocytes. *J. Physiol.* 509:67-80.
- Swillens, S., G. Dupont, L. Combettes, and P. Champeil. 1999. From calcium blips to calcium puffs: theoretical analysis of the requirements for interchannel communication. *Proc. Natl. Acad. Sci. USA.* 96:13750-13755.
- Tang, Y., and H. Othmer. 1995. Frequency encoding in excitable systems and its application to calcium oscillations. *Proc. Natl. Acad. Sci. USA.* 92:7869-7873.
- Tang, Y., J.L. Stephenson, and H. Othmer. 1996. Simplification and analysis of the models calcium dynamics based on IP_3 -sensitive calcium channel kinetics. *Biophys. J.* 70:246-263.

Thastrup, O., P. Cullen, B. Drobak, M. Hanley, and A. Dawson. 1990. Thapsigargin, A tumor promoter, discharges intracellular Ca^{2+} stores by specific inhibition of the endoplasmic reticulum Ca^{2+} ATPase. *Proc. Natl. Acad. Sci. USA.* 87:2466-2470.

Thomas, D., P. Lipp, M. J. Berridge, and M. D. Bootman. 1998. Hormone-evoked elementary Ca^{2+} signals are not stereotypic, but reflect activation of different size channel clusters and variable recruitment of channels within a cluster. *J. Biol. Chem.* 273:27130-27136.

Volpe, P., B. H. Alderson-Lang, and G. A. Nickols. 1990. Regulation of inositol 1,4,5-trisphosphate-induced Ca^{2+} release. I. Effect of Mg^{2+} . *American J. of Physiology.* 258:C1077-C1085.

Watras, J., I. Bezprozvanny, and B. E. Ehrlich. 1991. Inositol 1,4,5-trisphosphate-gated channels in cerebellum: presence of multiple conductance states. *J. Neurosci.* 11:3239-3245.

Tables and Figures

<u>Kinetic parameters</u>		<u>Other parameters</u>	
name	value	name	value
k_1	$12.0 (\mu\text{M} \times \text{s})^{-1}$	v_r	1.85
k_{-1}	8.0 s^{-1}	γ_0	0.1 s^{-1}
k_2	$23.4 (\mu\text{M} \times \text{s})^{-1}$	γ_1	20.5 s^{-1}
k_{-2}	1.65 s^{-1}	\hat{p}_1	$8.5 \mu\text{M} \times \text{s}^{-1}$
k_3	$2.81 (\mu\text{M} \times \text{s})^{-1}$	\hat{p}_2	$0.065 \mu\text{M}$
k_{-3}	0.21 s^{-1}	N	20

Table 1: Parameters values for the OTM.

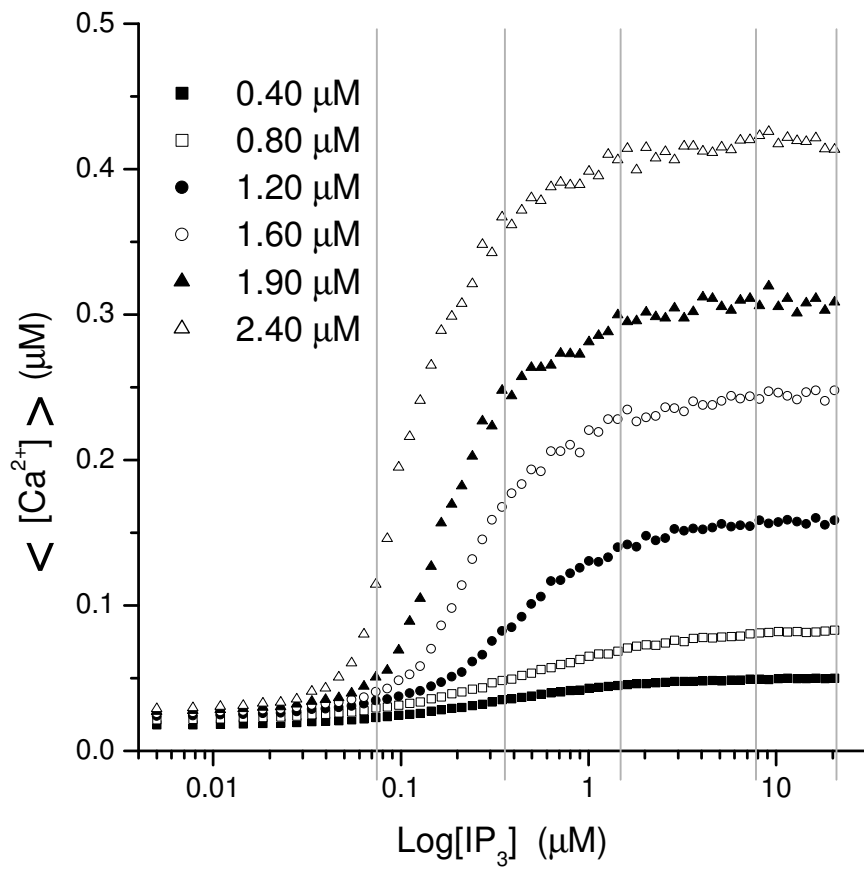


Figure 1: Mean value of $[Ca^{2+}]$ versus IP_3 concentration, for six different concentrations of the average intracellular calcium $[Ca^{2+}]_{ave}$, computed over 10,000 seconds.

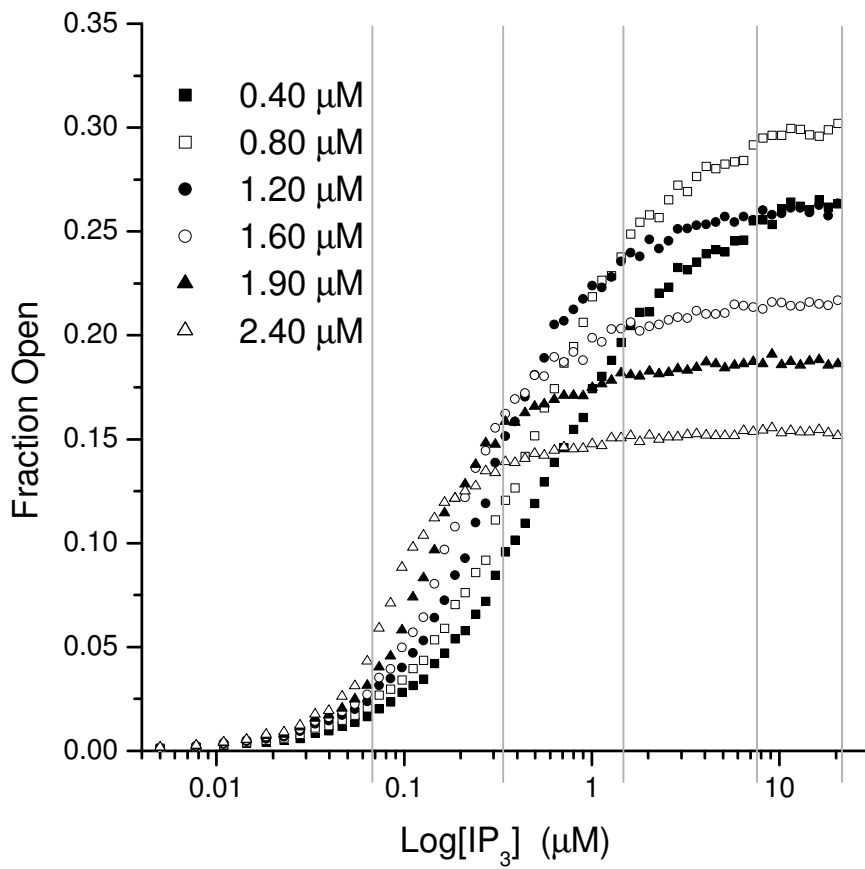


Figure 2: Fraction of open channels versus IP₃ concentration, for six different concentrations of the average intracellular calcium $[Ca^{2+}]_{ave}$, computed over 10,000 seconds.

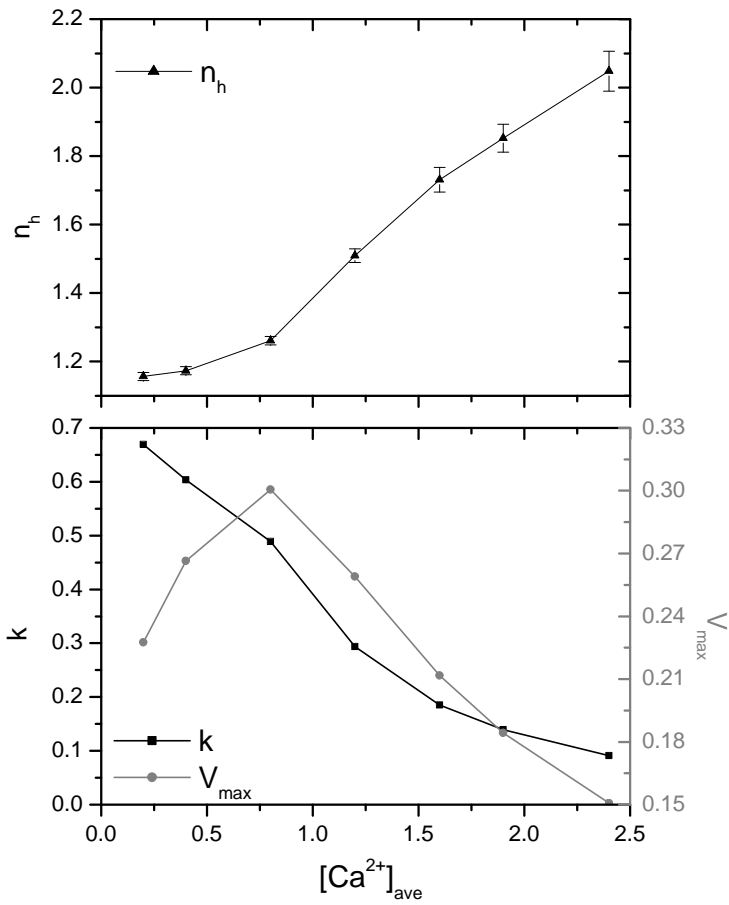


Figure 3: Top panel: Hill coefficient n_h for IP₃-induced calcium release versus $[Ca^{2+}]_{ave}$, obtained fitting data displayed in figure 2. Bottom panel: k and V_{max} values of the Hill curves for IP₃-induced calcium release versus $[Ca^{2+}]_{ave}$, obtained fitting data displayed in Fig. 2.

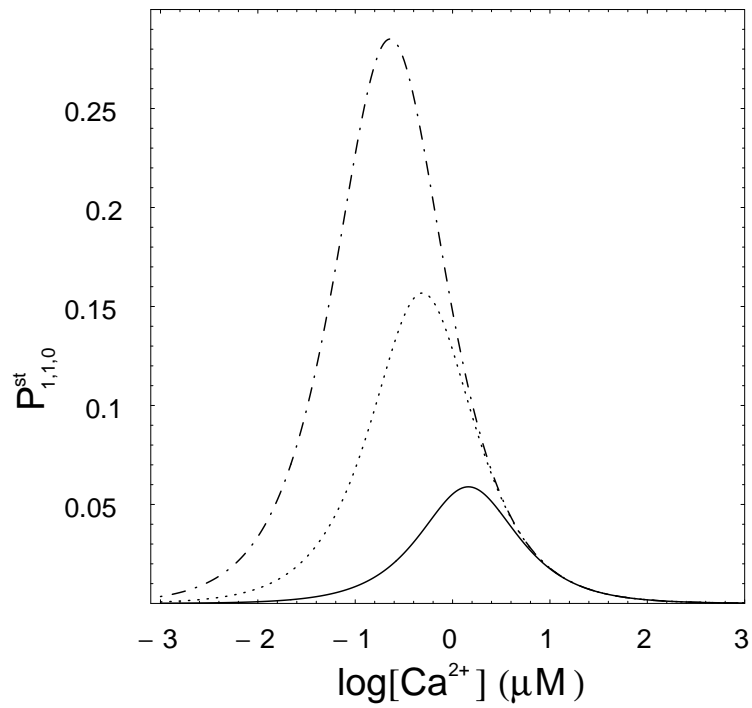


Figure 4: The theoretically predicted probability to find the open channel as a function of cytosolic $[\text{Ca}^{2+}]$ for three different values of IP_3 concentration (0.01 μM solid line, 0.1 μM dotted line, and 1 μM dot-dashed line).

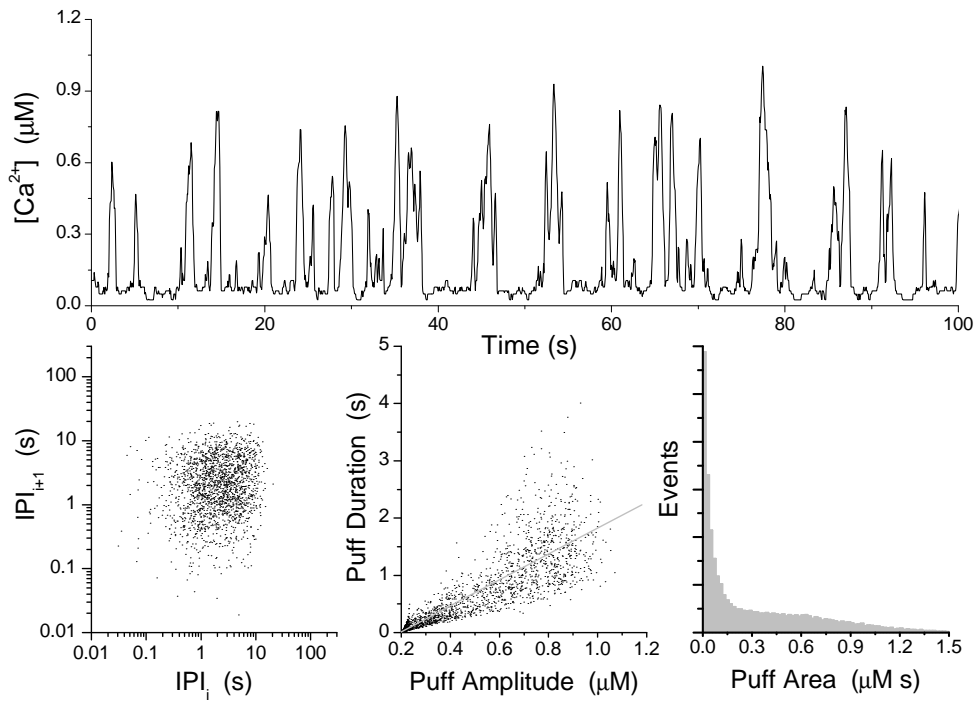


Figure 5: Top panel: 100 seconds of the stochastic temporal behavior of the calcium release from a cluster with 20 IP_3 Rs ($N = 20$, $[Ca^{2+}]_{ave} = 1.6$ and $IP_3 = 0.35$). Bottom-left panel: scatter plot of $IPI(i)$ versus $IPI(i+1)$ shown that there is not temporal correlation between two consecutive puffs. Bottom-center panel: scatter plot of puff amplitude versus puff duration shown that there is some correlation between puff durations and amplitudes of puffs. Bottom-right panel: puff area distribution shown that there is Ca^{2+} release of all sizes. All plots in the bottom panel were computed with puffs which amplitudes exceeds the threshold $0.20 \mu M$, recorded when simulate 10,000 seconds.

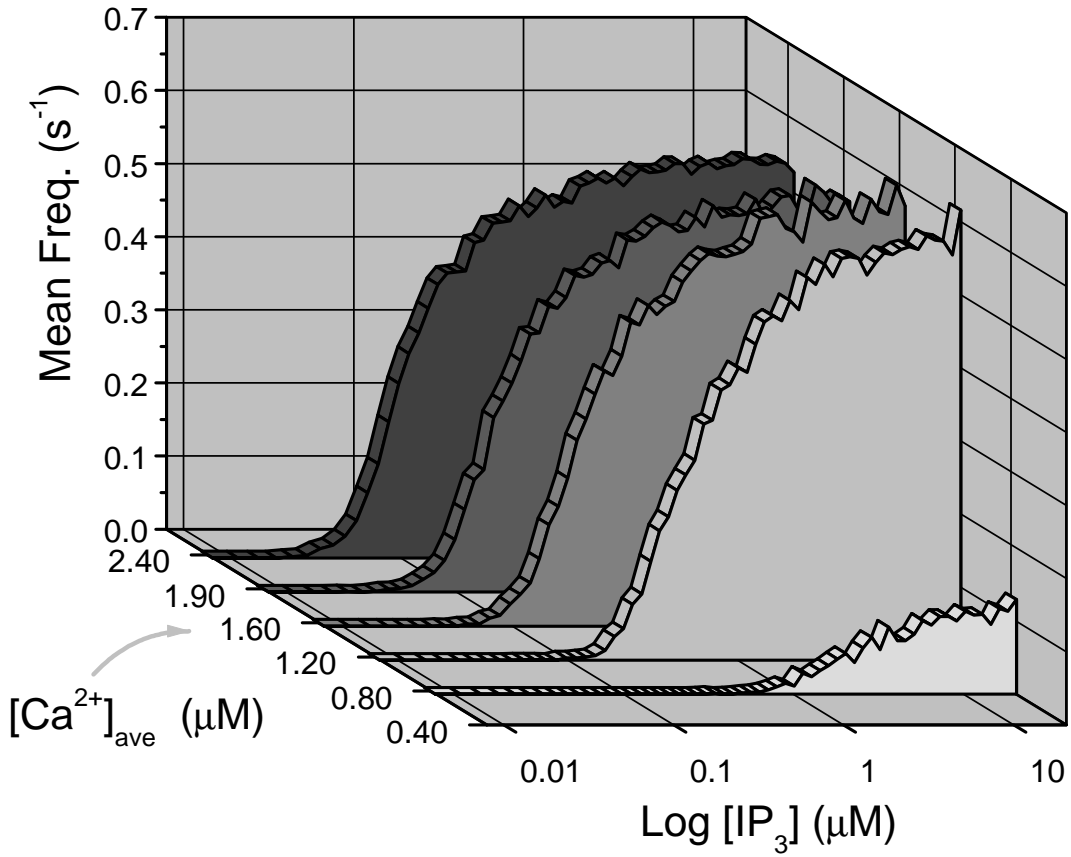


Figure 6: Mean frequency versus IP₃ concentration, for five different values of [Ca²⁺]_{ave}. All plots were computed with puffs which amplitudes exceeds the threshold 0.20 μM, recorded when simulate 10,000 seconds.

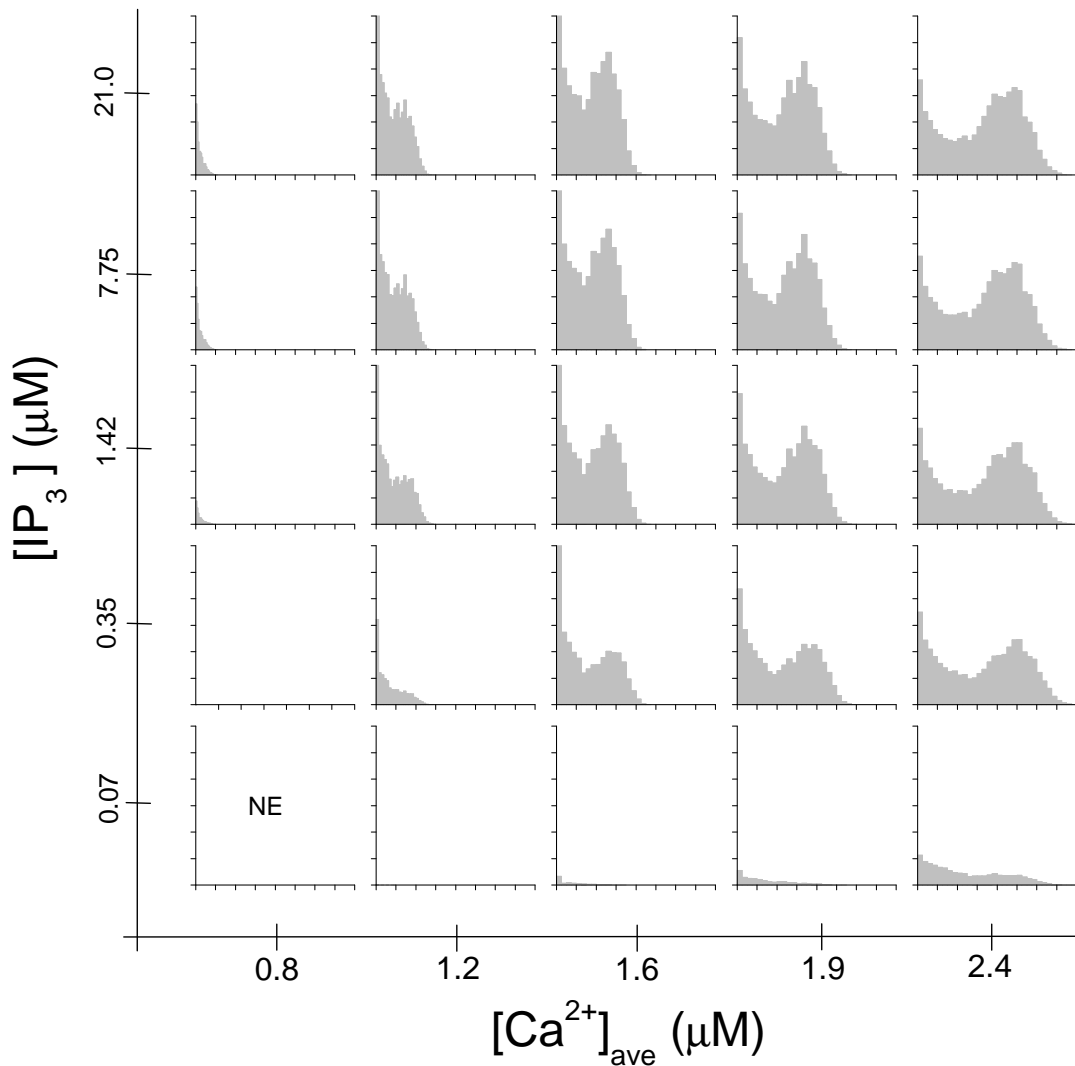


Figure 7: Diagram of the puff amplitude distributions is shown in the $[Ca^{2+}]_{ave}$ - IP_3 plane. The distributions was computed with all puffs, which amplitudes exceeds the threshold $0.20 \mu M$, recorded in 10,000 seconds. In this condition no events (NE) were recorded for $[IP_3]= 0.07 \mu M$ and $[Ca^{2+}]_{ave} = 0.8 \mu M$. The range of the axis are the same for all distributions, between $[0.20,1.8] \mu M$ for the amplitudes of puffs (horizontal axe), and between $[0,6000]$ for the number of events (vertical axe).

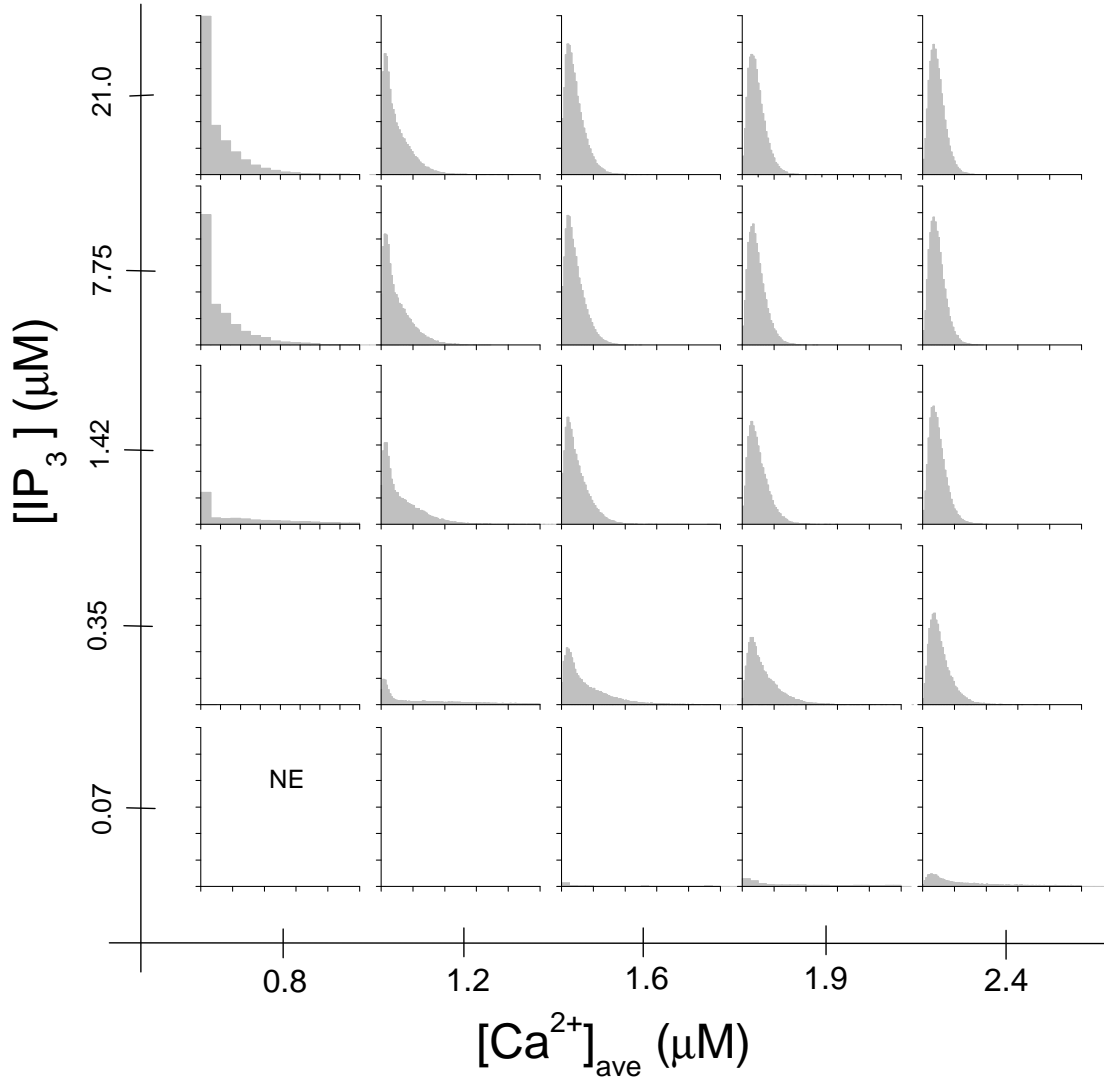


Figure 8: Diagram of the inter puff interval (IPI) distributions is shown in the $[Ca^{2+}]_{ave}$ - IP_3 plane. The distributions was computed with all puffs, which amplitudes exceeds the threshold $0.20 \mu M$, recorded in 10000 seconds. In this condition no events (NE) were recorded for $[IP_3]=0.07 \mu M$ and $[Ca^{2+}]_{ave} = 0.8 \mu M$. The range of the vertical axis are the same for all distributions, between $[0,6000]$ events. While the ranges of IPI (horizontal axis) are between $[0,80]$ seconds for the first column ($[Ca^{2+}]_{ave}=0.8 \mu M$), and between $[0,20]$ seconds in all other cases.

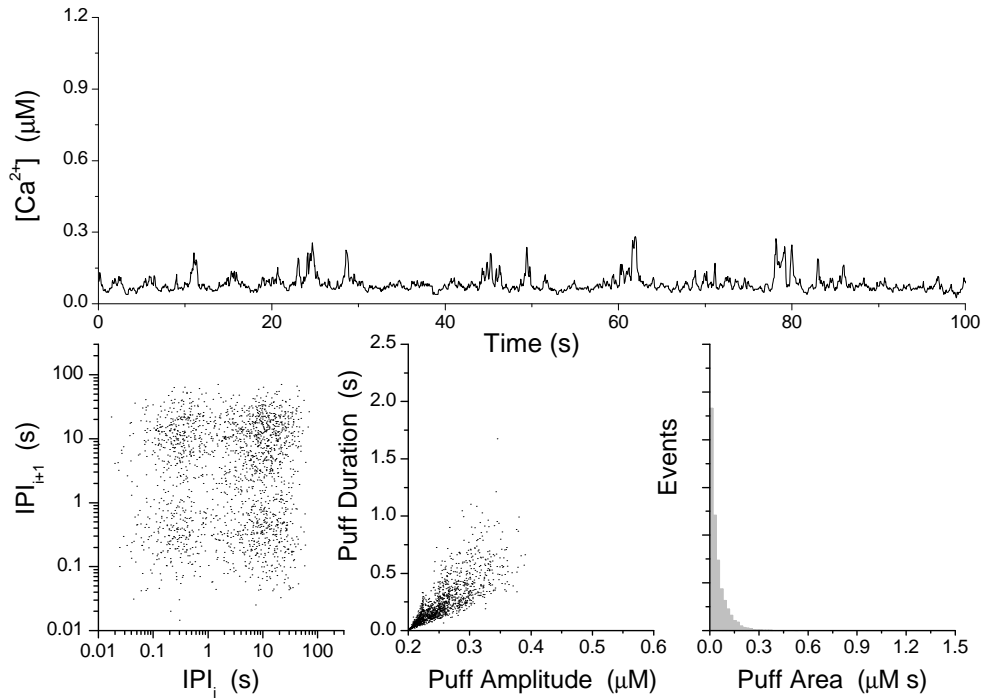


Figure 9: Top panel: 100 seconds of the stochastic temporal behavior of the calcium release from a cluster with 20 IP_3Rs ($N = 20$, $[Ca^{2+}]_{ave}=0.8 \mu M$ and $IP_3=21.0 \mu M$). Bottom-left panel: scatter plot of $IPI(i)$ versus $IPI(i + 1)$ shown that there is not temporal correlation between two consecutives puffs. Bottom-center panel: scatter plot of puff amplitude versus puff duration shown that there is some correlation between puff durations and amplitudes of puffs. Bottom-right panel: puff area distribution shown that there is Ca^{2+} release of all sizes. All plots in the bottom panel were computed with puffs which amplitudes exceeds the threshold $0.20 \mu M$, recorded in 10,000 seconds.

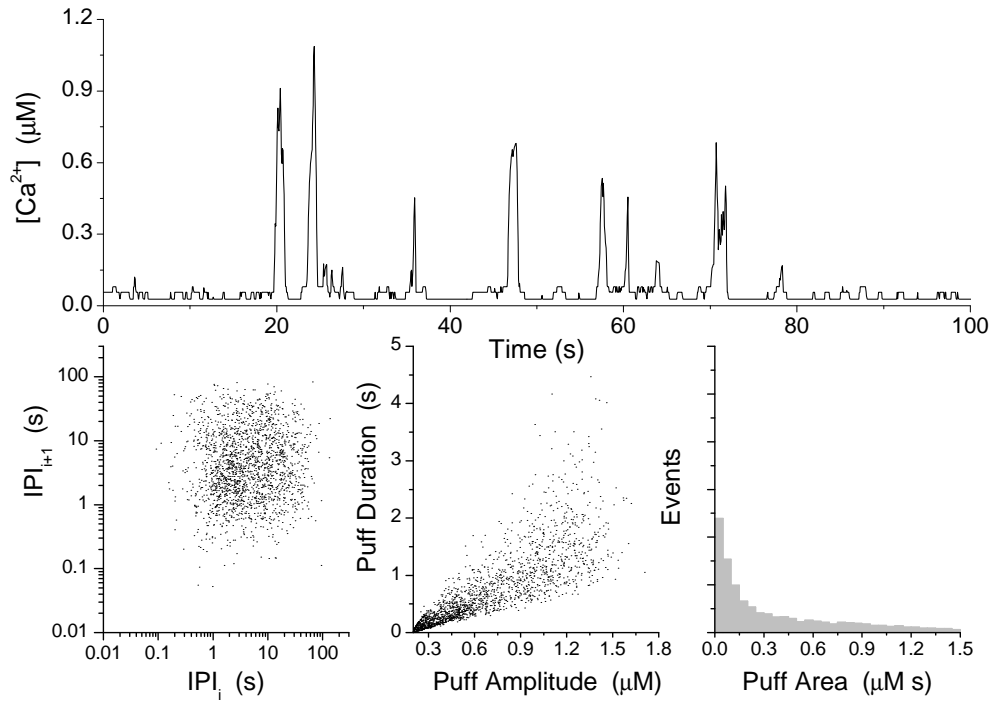


Figure 10: Top panel: 100 seconds of the stochastic temporal behavior of the calcium release from a cluster with 20 IP_3 Rs ($N = 20$, $[Ca^{2+}]_{ave} = 2.4 \mu M$ and $IP_3 = 0.07 \mu M$). Bottom-left panel: scatter plot of $IPI(i)$ versus $IPI(i + 1)$ shown that there is not temporal correlation between two consecutive puffs. Bottom-center panel: scatter plot of puff amplitude versus puff duration shown that there is some correlation between puff durations and amplitudes of puffs. Bottom-right panel: puff area distribution shown that there is Ca^{2+} release of all sizes. All plots in the bottom panel were computed with puffs which amplitudes exceeds the threshold $0.20 \mu M$, recorded in 10,000 seconds.